

Anatomic three-dimensional model-assisted surgical planning for treatment of pediatric hip dislocation due to osteomyelitis

Journal of International Medical Research

48(2) 1–9

© The Author(s) 2019

Article reuse guidelines:

sagepub.com/journals-permissions

DOI: 10.1177/0300060519854288

journals.sagepub.com/home/imr



Yi-Ping Wei¹, Yu-Cheng Lai² and Wei-Ning Chang³ 

Abstract

Management of pediatric septic coxarthrititis and osteomyelitis of the femur is challenging, and the sequelae of multiplanar hip joint deformity with instability are difficult to reconstruct. The inadequacy of a suitable device for fixing small bones during pediatric osteotomy is a hindrance to the correction of subluxated hip joints and deformed femurs in children. Two-dimensional axial images and three-dimensional (3D) virtual models representing the patient's individual anatomy are usually reserved for more complex cases of limb deformity. 3D printing technology can be used for preoperative planning of complex pediatric orthopedic surgery. However, there is a paucity of literature reports regarding the application of 3D-printed bone models for pediatric post-osteomyelitis deformity. We herein present a case of a 4-year-old boy who underwent treatment for post-osteomyelitis deformity. We performed corrective surgery with Pemberton osteotomy of the right hip, multilevel varus derotation osteotomy of the right femur, and immobilization with a hip spica cast. A 3D-printed bone model of this patient was used to simulate the surgery, determine the proper osteotomy sites, and choose the appropriate implant for the osteotomized bone. A satisfactory clinical outcome was achieved.

Keywords

Pediatric, hip dysplasia, femur, deformity correction, 3D printing, surgical planning and simulation

Date received: 25 December 2018; accepted: 10 May 2019

¹Department of Orthopaedic Surgery, Kaohsiung Veterans General Hospital, Kaohsiung, Taiwan, R.O.C.; National Defense Medical Center, Taipei, R.O.C.

²Department of Orthopaedic Surgery, Kaohsiung Veterans General Hospital, Kaohsiung, Taiwan, R.O.C.; National Yang Ming University, Taipei, R.O.C.

³Department of Orthopedics, Kaohsiung Veterans General Hospital, Kaohsiung, Taiwan, R.O.C.; Department of Orthopedic Surgery, School of Medicine, National Yang Ming University, Taipei, Taiwan, R.O.C.

Corresponding author:

Wei-Ning Chang, Department of Orthopedics, Kaohsiung Veterans General Hospital, No. 386 Dazhong 1st Road, Zuoying District, Kaohsiung City 81362, Taiwan (R.O.C.). Email: wncchang@vghks.gov.tw



Introduction

Correction of pediatric skeletal dysplasia is a procedure with high aesthetic and functional demand. Therefore, meticulous surgical planning is necessary. Both two-dimensional axial images and three-dimensional (3D) virtual models representing the patient's individual anatomy are used for more complex limb deformities.¹ This processed digital information can assist orthopedic surgeons in preparing patient-specific procedures. The use of 3D-printed models as surgical "guides" shows great promise. However, there is a paucity of reports regarding the application of 3D-printed models for pediatric post-osteomyelitis deformity. Using the methodology detailed in the present case report, an inexpensive 3D skeletal model (about USD582.37 in this case) was used as a preoperative surgical guide for skeletal reconstruction. Suitable implants can be pre-bent or custom-made according to the 3D model.¹ A more precise correction angle and cutting site in pediatric cases can also be attained.

Case report

This case involved a first-born boy who was delivered in a physically normal state. He presented with a limping gait at 4 years of age. Bone changes were detected on radiography and magnetic resonance imaging, with lobulated joint effusion over the right hip joint and peripheral enhancement. Radiologists and an orthopedic surgeon interpreted the lesion, and a diagnosis of osteomyelitis was made. Antibiotic administration and surgical intervention were initiated because of the rapid clinical progression.

Six debridement and open arthrotomy procedures using the lateral and direct anterior approach were performed. The patient's right leg was immobilized in a ReBorn Essence external skeletal fixator

(BAUI Biotech, Taipei, Taiwan), and he was treated with the induced membrane technique (Masquelet procedure) to reconstruct the bone length after the infection had subsided. Repeated radiographs showed a proximal femur valgus deformity with lateral subluxation of the right femoral head and posterior angulation of the femoral shaft at the middle third, with a nearly full osseous recovery (Figure 1(a)).

3D planning

The clinical examination and 3D computed tomography (CT) image revealed a genu valgus deformity with flexion and extension deficits. A further corrective surgery for the angulation and rotation was scheduled for the patient. 3D CT imaging was performed for qualitative and quantitative analyses of the bone tissue (Figure 1(b) and (c)) and planning for the correction. A proximal femur varus derotation osteotomy was carried out to correct the angulation and rotation of the femoral shaft, and a Pemberton osteotomy was performed for the residual acetabular dysplasia with lateral subluxation of the right femoral head.

Although virtual positioning could be guided by 3D CT imaging, a more precise osteotomy and implant positioning could be achieved with the help of a life-size model. The surgical plan in this case was created and patient-specific guidance was provided with the collaboration of an experienced orthopedic consulting firm specializing in 3D orthopedics and patient-specific instrumentation (Figure 2(a)).

3D simulation with 3D prints

A model based on the mirror image of the relatively healthy leg was used to represent the original anatomy and alignment. The deformity was better visualized by comparing it with the unaffected limb. Simulations of possible osteotomy options

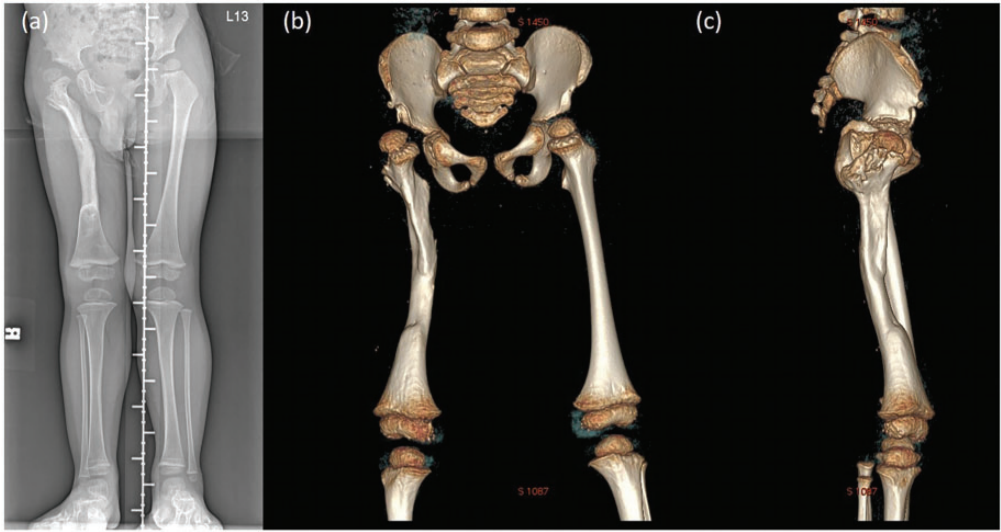


Figure 1. Radiographs taken before corrective surgery. (a) Triple film showing the proximal femur deformity with osseous recovery. Three-dimensional computed tomography image: (b) anteroposterior and (c) lateral views

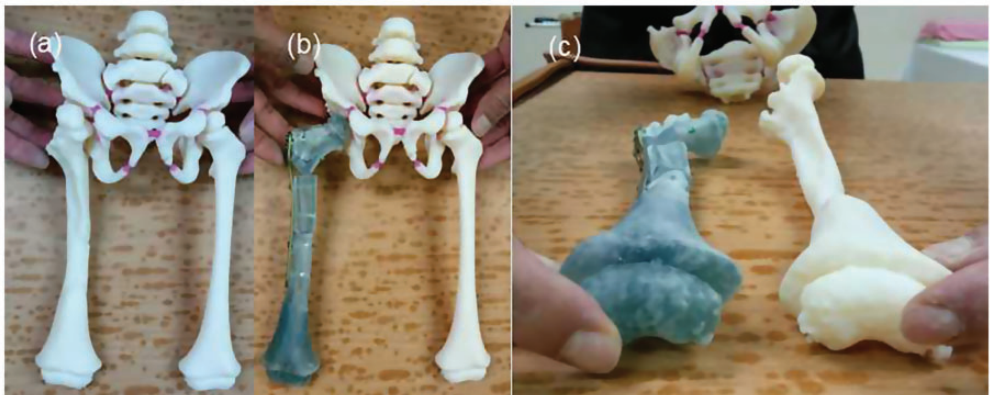


Figure 2. Customized-to-patient three-dimensionally-printed guide. (a) The patient-specific guide for our patient. (b) Two resecting osteotomies can achieve optimal joint congruency and varus angle correction. (c) Correcting the femoral rotation would result in joint translation in both the coronal and axial planes

were done on the model and the results were observed (Figure 2(b) and (c)). After a few osteotomy options had been analyzed, one osteotomy cut was made vertically to the femoral shaft on the subtrochanteric area, and another was made on the middle third of the femur to correct the bowing deformity

of the midshaft. Correction of femoral rotation can result in either joint translation in the coronal and axial planes or difficulty with fixation, both of which could be prevented with the help of the 3D model in the present case. The result of the planned osteotomy showed good bone contact and

elimination of the genu valgus deformity. Another osteotomy was performed superior to the anterior superior iliac spine and advanced forward medial to the acetabular wall under image intensifier guidance, aiming at the triradiate cartilage.

The surgery involved a planned Pemberton osteotomy of the right hip and a varus derotation osteotomy of the right femur. A locking proximal humeral plate (DePuy Synthes, West Chester, PA, USA) was chosen based on the preoperative simulation.

3D model-assisted surgery

The preoperative plan included reaching optimal joint congruency, determining the correction angle, and restoring the length of the femoral shaft. When simulating the operative procedure with the life-sized 3D model, we mostly emphasized optimal joint congruency and coverage of the acetabulum. First, an osteotomy was made over the metaphyseal site of the proximal femur and fixed with the chosen locking plate to correct the subluxated femoral head. To correct the coexisting bowing deformity of the femoral shaft, another osteotomy was created distal to the first cut, guided by the locking plate to ensure that at least three screws were fixed at the distal end. With the help of the 3D model, we were

able to optimize the osteotomy site and the correcting angle on the life-sized simulating system. Another advantage of 3D model simulation was comparison with the unaffected limb, which is extremely difficult to achieve during the operation considering the decubitus position. After correction of the bowing deformity, the 5-mm leg length discrepancy was accurately measured and corrected by midshaft shortening.

After the simulation process, the exact osteotomy sites according to the distance from the tip of the greater trochanter, the correcting angle, and the accurate leg length discrepancy were recorded and applied to the surgery. After obtaining C-arm verification, the osteotomy line was perfectly matched with the preoperative plans and alignment, and plate-and-screw fixation was performed to finish the procedure (Figure 3(a) and (b)). A postoperative hip spica was applied with the hip joint in 20° flexion, 40° abduction, and 10° internal rotation. The resulting femoral segment was flipped 30° in the coronal plane.

Postoperative follow-up

Because the osteotomy achieved the best possible bone fixation, the patient was encouraged to start passive joint mobilization and stretching exercises 4 months after



Figure 3. Postoperative (a) anteroposterior and (b) lateral views. Fifteen-month postoperative (c) anteroposterior and (d) lateral views

the surgery, and he underwent a series of hip spica corrections. We compared the radiological and physical findings before and after the surgery (Table 1). Osteotomy site union was confirmed during the 15-month follow-up (Figure 3(c) and 3(d)). Because of residual external rotation contracture of the extended hip with toe-out gait, we suggested the use of a twister cable based on a video analysis. Additionally, the leg length discrepancy was <5 mm at the 2-year postoperative follow-up (Figure 4).

Written informed consent was obtained from the patient's legal guardian for the publication of this case report. This study was approved by the Institutional Review Board of the Kaohsiung Veterans General Hospital.

Discussion

Traditional skeletal corrections rely mostly on two-dimensional radiographs to create a preoperative plan, and preoperative precision or tools with which to perform the plan are sometimes lacking. Thus, such surgeries are highly dependent upon use of the C-arm. Postoperative complications, including malalignment, residual deformity,

and implant failure, are common.¹⁻³ Superior precision in 3D printing technology provided a customized osteotomy guide for the treatment of an 18-year-old male



Figure 4. Triple film at 2-year postoperative follow-up showing no significant leg length discrepancy (<0.5 cm)

Table 1. Physical function and radiological parameters before and after surgery

	Physical function			Radiological parameters	
	Gait	Squat	Range of motion of affected hip	Acetabular index	Center-edge angle of Wiberg
Preoperative performance	Trendelenburg gait Foot progression angle: 10° of external rotation/neutral (right/left)	Unavailable	Hip abduction: $70^\circ/70^\circ$ (right/left); knee flexion: $0^\circ-140^\circ/0^\circ-140^\circ$ (right/left); bilateral thigh-foot angle: neutral; hip internal/external rotation: $10^\circ/30^\circ$ (right) and $50^\circ/50^\circ$ (left)	24.39°	22.96°
Postoperative performance (1 follow-up)	No Trendelenburg gait	Able to squat to full depth	Only changes in hip internal/external rotation angle: $10^\circ/80^\circ$ (right) and $50^\circ/45^\circ$ (left)	15.65°	25.76°

patient with a 40° cubitus varus deformity due to a right humeral supracondylar fracture.¹ Correction with 3D images and 3D-printed models helps surgeons to accomplish correction with results that are identical to the plan.¹

In pediatric orthopedics, joint function is more important than joint appearance. In the present case, we recorded the preoperative joint function for comparison with the postoperative performance (Table 1). The range of motion of the hip and knee joints was measured 1 day before the operation and 1 year after the completion of the corrective surgery. All measurements were performed by the same examiner (one senior orthopedic surgeon) using the same protocols. Significant alterations were noted because of the concentrically reduced femoral head, greater acetabular opening, and soft tissue releasing procedures, which had been initially performed from the inferomedial direction of the hip joint.

Before correction, analysis of our patient's video record revealed a trunk shift over the affected leg and a decreased stance time on the affected side. Because no significant leg

length discrepancy (<0.5 cm) was present on the radiograph, we believed that the combined effects of the hip instability and the surrounding scar tissue were likely the main causes of his Trendelenburg gait.

The difference between the patient's preoperative and postoperative stance was compared (Figures 5 and 6). When taking the photographs, we asked him to stand evenly on both feet without leaning against the wall. We observed significant shifting of his body center and external rotation of his right knee joint when standing before corrective surgery.

We performed a preoperative and 1-year postoperative evaluation of the patient's acetabular development by measuring radiological parameters such as the acetabular index and the center-edge angle (CEA) of Wiberg (Table 1). A higher acetabular index may be associated with a greater risk of hip dysplasia or subluxation.⁵ The CEA is another radiological parameter that indicates the harmony between the femoral head and the acetabulum. In our case, the postoperative CEA was higher than the preoperative value. A higher CEA



Figure 5. Photographs taken before the corrective surgery. (a) Front view. (b) Right-side view. (c) Back view. (d) Left-side view

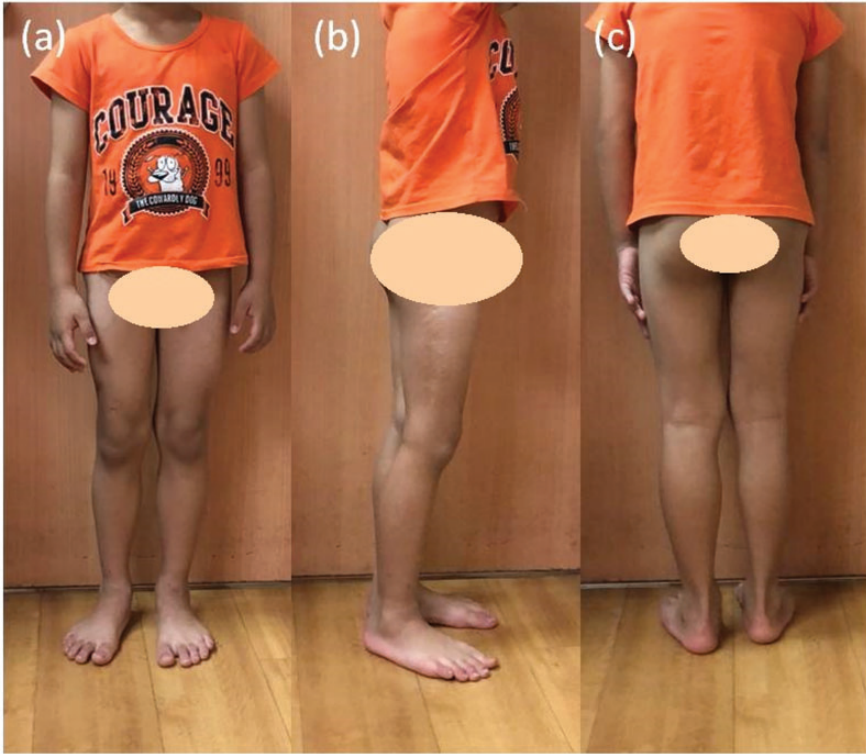


Figure 6. Photographs taken at the 2-year postoperative follow-up. (a) Front view. (b) Right-side view. (c) Back view

reflects a larger femoral head and a more developed acetabulum, indicating excellent coverage of the femoral head.⁵ The result of our case suggests that the use of 3D printing models improves the postoperative performance as shown by both physical function and radiological evidence.

However, we observed residual external rotation contracture of the extended hip in our patient after the correction. Inadequate tightening of the medial hip capsule at the end of the operation may have been the main cause. It was difficult to measure the tolerance of the soft tissue by the preoperative 3D model. Our study revealed a limitation of this technology: it can only provide a model of bones and does not consider the impact of soft tissue, which differs greatly from the real operative situation.

After examining our patient's gait at follow-up, a twister cable was indicated for conservative correction. The hip joint was connected to a pelvic band with a flexible rod set in an overcorrected position, and the two components were held together with set screws. This design was meant to decrease the torque on the knee caused by rotation. The patient returned for follow-up every 6 months.

Previous research indicates that 3D printing technology might shorten the operation time.^{6,7} A randomized trial published in 2019 evaluated the efficacy of the use of 3D models in cases of distal radial fracture.⁶ The mean operative time was significantly shorter by 9 minutes in the 3D model group than in the routine treatment group (66.5 ± 5.3 vs. 75.4 ± 6.0 minutes, respectively;

$P < 0.001$). One systematic review published in 2016 showed that the use of a 3D model resulted in a shorter operation time.⁷ The fracture or deformity prototype can increase the surgical efficiency and reduce the operation time.

With the development of 3D technology-assisted surgery, new advancements for treatment of limb deformities and fractures in the field of pediatric orthopedics are constantly appearing. One study published in 2019 evaluated the clinical use of 3D printing in pediatric fractures requiring immobilization.⁸ Eighteen children wore their 3D devices in 12 to 24 h. The results of the study indicated that the use of a 3D device instead of a traditional plaster cast can be an effective treatment of pediatric nondisplaced metaphyseal distal radius fractures, with high overall patient satisfaction.⁸ We believe that 3D technology could be extended to the treatment of more complex fractures in the future. One systemic review published in 2019 introduced software systems that calculate the deformity parameters for external fixation to treat leg length discrepancies with concomitant angular and/or rotational deformities.⁹ The application of gene therapy and tissue-engineered scaffolds to bone repair was also mentioned. Alluri et al.¹⁰ loaded human adipose-derived stem cells that had been virally transduced to produce bone morphogenetic protein 2 onto a 3D-printed scaffold consisting of hyperelastic bone. This novel composite material has clinical potential to treat skeletal defects. The composite is a highly osteoconductive 3D scaffold that delivers transduced human cells with a highly osteoinductive signal.

The use of a 3D-printed patient-specific guide is a safe, modern, affordable, and promising method that offers advantages including a shorter surgical time, optimally positioned implant placement, acceptable alignment, and a probable lower rate of complications.⁷ The utilization of

3D-printed models for skeletal deformity surgery, especially complex and difficult pediatric surgery, provides superior precision and foreseeably better outcomes. We strongly believe that with the promotion of 3D printing methodology, models for preoperative planning may soon become the gold standard for pediatric deformity correction surgery.

Declaration of conflicting interest

The authors declare that there is no conflict of interest.

Funding

This research received no specific grant from any funding agency in the public, commercial, or not-for-profit sectors.

ORCID iD

Wei-Ning Chang  <https://orcid.org/0000-0003-4507-0064>

References

1. Gemalmaz HC, Sariyilmaz K, Ozkunt O, et al. A new osteotomy for the prevention of prominent lateral condyle after cubitus varus correctional surgery-made possible by a 3D printed patient specific osteotomy guide: a case report. *Int J Surg Case Rep* 2017; 41: 438–442.
2. Makridis KG, Theocharakis S, Fraggakis EM, et al. Reconstruction of an extensive soft tissue and bone defect of the first metatarsal with the use of Masquelet technique: a case report. *Foot Ankle Surg* 2014; 20: e19–e22.
3. Gouron R, Deroussen F, Plancq MC, et al. Bone defect reconstruction in children using the induced membrane technique: a series of 14 cases. *Orthop Traumatol Surg Res* 2013; 99: 837–843.
4. Hedequist D, Bishop J and Hresko T. Locking plate fixation for pediatric femur fractures. *J Pediatr Orthop* 2008; 28: 6–9.
5. Sarikaya B, Sipahioglu S, Sarikaya Z, et al. The early radiological effects of Dega and Pemberton osteotomies on hip development

- in children aged 4–8 years with developmental dysplasia of the hip. *J Pediatr Orthop B* 2017; 27: 250–256.
6. Chen C, Cai L, Zheng W, et al. The efficacy of using 3D printing models in the treatment of fractures: a randomised clinical trial. *BMC Musculoskelet Disord* 2019; 20: 65.
 7. Tack P, Victor J, Gemmel P, et al. 3D-printing techniques in a medical setting: a systematic literature review. *BioMed Eng Online* 2016; 15: 115.
 8. Guida P, Casaburi A, Busiello T, et al. An alternative to plaster cast treatment in a pediatric trauma center using the CAD/CAM technology to manufacture customized three-dimensional-printed orthoses in a totally hospital context: a feasibility study. *J Pediatr Orthop B* 2019; 28: 248–255.
 9. Iobst C. New technologies in pediatric deformity correction. *Orthop Clin North Am* 2019; 50: 77–85.
 10. Alluri R, Jakus A, Bougioukli S, et al. 3D printed hyperelastic “bone” scaffolds and regional gene therapy: a novel approach to bone healing. *J Biomed Mater Res A* 2018; 106A: 1104–1110.